

DTIC FILE COPY

2

NASA
Technical
Paper
3063

AD-A231 724

AVSCOM
Technical
Report
90-C-001

**Experimental and Analytical
Evaluation of Efficiency of
Helicopter Planetary Stage**

November 1990

Timothy L. Krantz

DTIC
ELECTE
FEB 20, 1991
S B D



DISTRIBUTION STATEMENT A

**Approved for public release
Distribution Unlimited**

NASA

91 2 14 057

**NASA
Technical
Paper
3063**

**AVSCOM
Technical
Report
90-C-001**

1990

**Experimental and Analytical
Evaluation of Efficiency of
Helicopter Planetary Stage**

Timothy L. Krantz
*Propulsion Directorate
USAARTA-AVSCOM
Lewis Research Center
Cleveland, Ohio*



National Aeronautics and
Space Administration
Office of Management
Scientific and Technical
Information Division

Summary

The mechanical efficiency of a helicopter transmission planetary stage was studied. Experiments were done by using two identical planetary stages in a back-to-back, test-and-slave arrangement with separate lubrication systems. A total of 124 different conditions were tested. The parameters varied were speed, torque, type of lubricant, lubricant system temperature, and lubricant flow rate. Experimentally measured efficiency ranged from 98.64 to 99.83 percent depending on the operating conditions.

The performance of the planetary stage was also studied analytically. The test hardware and conditions were modeled and analyzed by using computer programs that predict power losses from gear meshes, from gear windage, and from planet bearings. Two different models for calculating power loss due to oil displacement from the gear mesh were also studied, and the results were included in the analytical predictions of efficiency.

The experimental results were compared with the analytical predictions. The analysis predicted higher efficiencies than were measured experimentally. The results of this study showed trends similar to those of previous investigations.

Introduction

The power loss of gears, bearings, and transmissions has been studied by many investigators (refs. 1 to 11). Many operating conditions and design factors influence the efficiency of a gearbox. References 1 to 4 report the results of experiments done to study the effects of operating conditions, such as load, speed, and lubrication method, on gear performance. The studies of references 1 and 5 indicate that the type of lubricant used in a gearbox has a large effect on the gearbox efficiency. In references 6 to 8 analytical methods are developed and used to study the effects of gear design parameters, such as contact ratio and nonstandard tooth designs, on power loss. Examples of studies on special aspects of gear performance are reference 2, on churning loss; reference 3, on the performance of high-speed gears; and reference 4, on the efficiency of a planetary reduction stage.

Helicopter transmission efficiencies are extremely high, typically above 95 percent for the complete helicopter main rotor transmission. However, slight changes in efficiency can affect the complete transmission system. Changes in transmission operating parameters (e.g., the amount of

lubricant needed or the operating temperature) can affect oil cooler size and thus transmission weight. Improving the efficiency will lower fuel usage and thus increase payload or aircraft range.

Reference 4 describes an analytical and experimental study of the efficiency of a planetary stage with a four-planet configuration from an Army OH-58 helicopter. It includes the results of a parametric study of how operating conditions affect a planetary stage's mechanical efficiency. The research described herein was a continuation of that study.

The objectives of the present investigation were to study the performance of a planetary reduction stage and to improve the analytical methods used to predict the power loss from a gear train. A planetary stage with a three-planet configuration from an Army OH-58 helicopter was studied. The planetary stage was tested to a maximum of 239 kW (320 hp) in a back-to-back, closed-loop test rig. A parametric study was done to experimentally determine the effects of operating conditions on performance. The planetary stage was also studied analytically by using techniques similar to those of reference 4. The analytical techniques used in reference 4 did not account for the power loss due to oil trapped by the gear teeth being displaced as the gears meshed. These displacement losses were identified as a possible explanation of the differences between the experimental results and the analytical predictions of that study. In the research described herein, two different models to account for these displacement losses were developed and studied. The results from this research were compared with the results of previous studies.

Experimental Apparatus and Procedure

Test Rig, Instrumentation, and Data Acquisition System

The test rig contained two identical planetary stages that were driven back to back. The planetary stages, described in table I, were from the U.S. Army's OH-58 helicopter main rotor transmission (fig. 1). This transmission has a reduction ratio of 17.44 overall, with the planetary stage contributing a ratio of 4.667. The planet gear carrier, the planet gears, and the sun gear used in the program are shown in figure 2. The assembled carrier contained the planet gears, the planet bearings, the planet bearing posts, and the mechanical connection to the output shaft. Each planetary stage contained three planet gears.

TABLE I.—PLANETARY GEAR TRAIN HARDWARE USED IN TEST AND SLAVE SECTIONS

[Planetary reduction ratio, 4.667. Planet bearing data (double-row spherical): inside diameter, 31.8 mm (1.25 in.); outside spherical diameter, 76.2 mm (3.00 in.); roller diameter, 13 mm (0.512 in.); number of rollers per row, 12.]

Gear	Number of teeth	Module, mm	Diametral pitch, in. ⁻¹	Pressure angle, deg	Pitch diameter	
					mm	in.
Sun	27	2.868	8.857	24.6	77.4	3.048
Planet	35	2.868	8.857	24.6	100.4	3.952
Ring	99	2.778	9.143	20.2	275.0	10.828

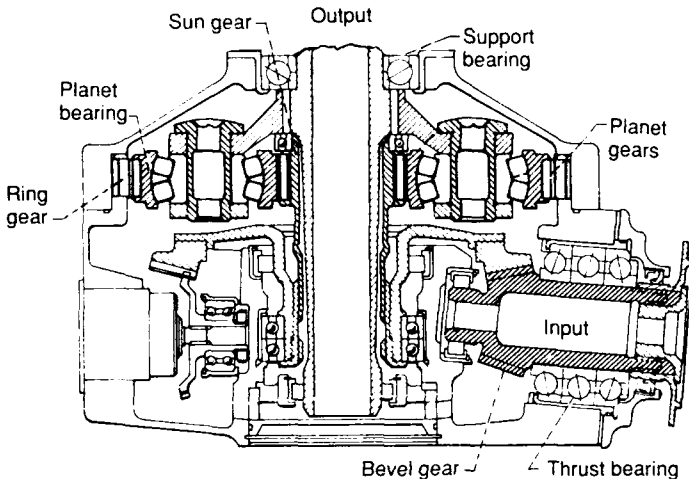
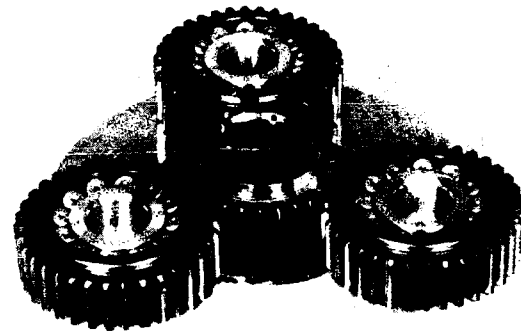


Figure 1.—Cross section of OH-58 helicopter transmission.



C-89-13344

Figure 2.—Sun gear, planet gears, and carrier used in test program.

The test rig (fig. 3) was a regenerative-torque, back-to-back configuration where a test and a slave section were loaded against each other by applying hydraulic pressure to a rotating torque actuator. The rotating torque actuator twisted the slave-section sun gear relative to the high-speed shaft to produce the loop torque. The drive motor rotated the high-speed shaft and supplied power to overcome rig and test hardware losses. The entire rig and its lubrication system were insulated during testing so that test temperatures could be reached in a reasonable amount of time.

Each planetary section was lubricated by separate, identical systems. Each system included a number of manifolds through which flow was dispersed to individual areas. The three lubricated areas in each section were the sun-planet mesh, the planet-ring mesh, and the planet bearing area. Turbine flowmeters measured the total flow to each section and the flow to each of the three lubricated areas. Each lubrication system was also instrumented with thermocouples and pressure transducers. Figure 4 shows the typical orientation of the lubrication jets in relation to the test hardware.

The input torque to the rig was measured by a commercially available transformer-coupled torquemeter. The torques carried by the low-speed shaft and by the high-speed shaft were

measured with strain gages arranged in a full Wheatstone bridge on the shafts. The Wheatstone bridge conditioning circuits rotated with the shafts, and the output from the circuits was transmitted across slip rings. The output signals from the torque-measuring instruments were low-pass filtered to remove frequencies above 0.2 Hz. Filtering yielded a time-averaged torque instead of the instantaneous torque that the instruments could measure.

Data were collected and stored by a remote mainframe computer to provide a chronological history of the test and to enable post-test processing of key data. All data channels were updated every 2 sec while tests were being run.

Reference 4 gives a more detailed description of the test rig, the instrumentation, and the calibration methods.

Test Rig Tare Losses

The test rig tare losses are those due to components other than the gear meshes and the planet bearings. The rig as shown in figure 3 requires a number of bearings and seals that are not part of the helicopter transmission's planetary stage to support shafts and to allow operation in the regenerative loop manner. Power losses are also attributed to the two slip rings used. Reference 4 reports the results of experiments done to measure the tare loss associated with bearings, seals, and slip

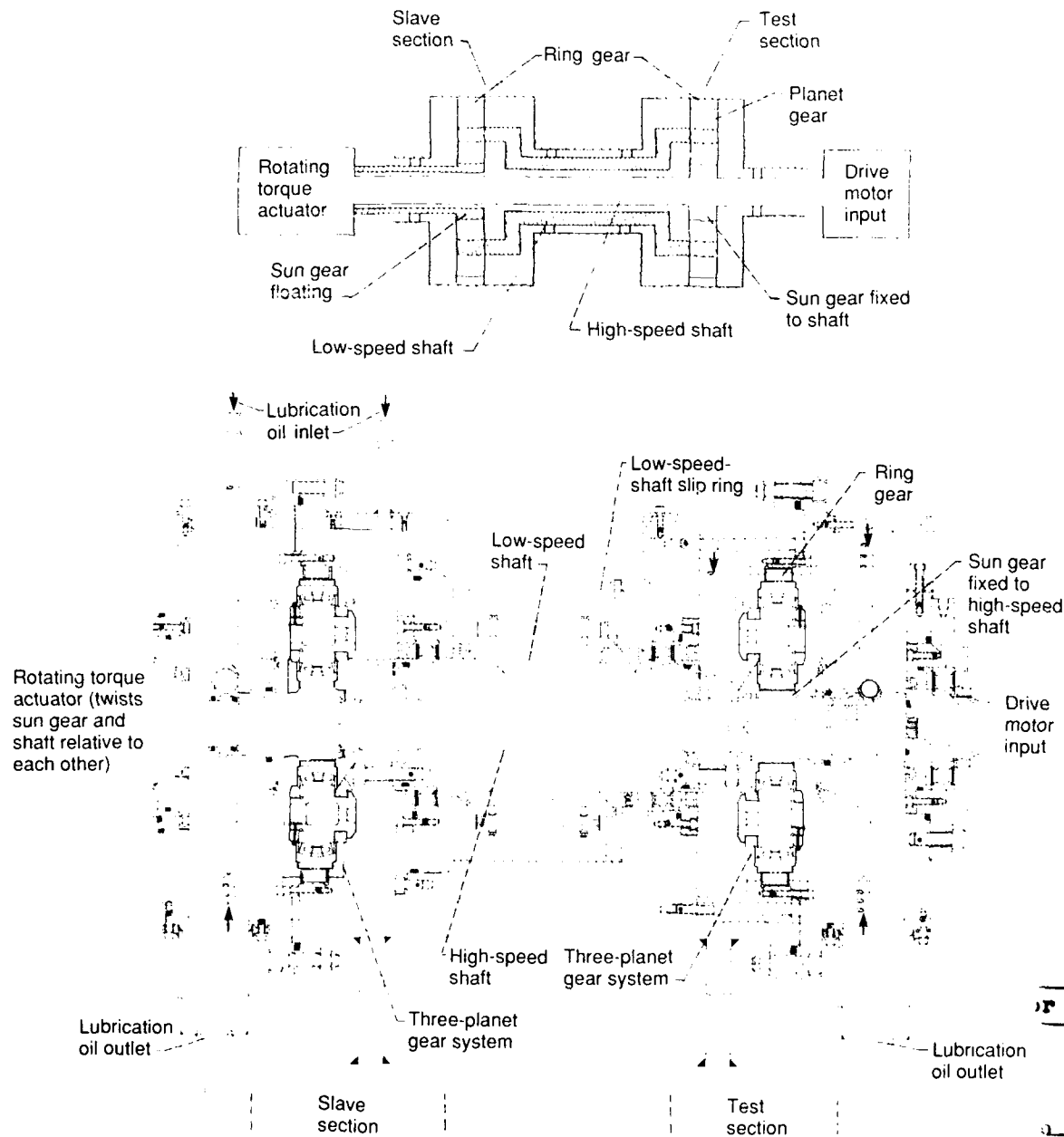


Figure 3.—Cross-sectional view of test gearbox showing key components.

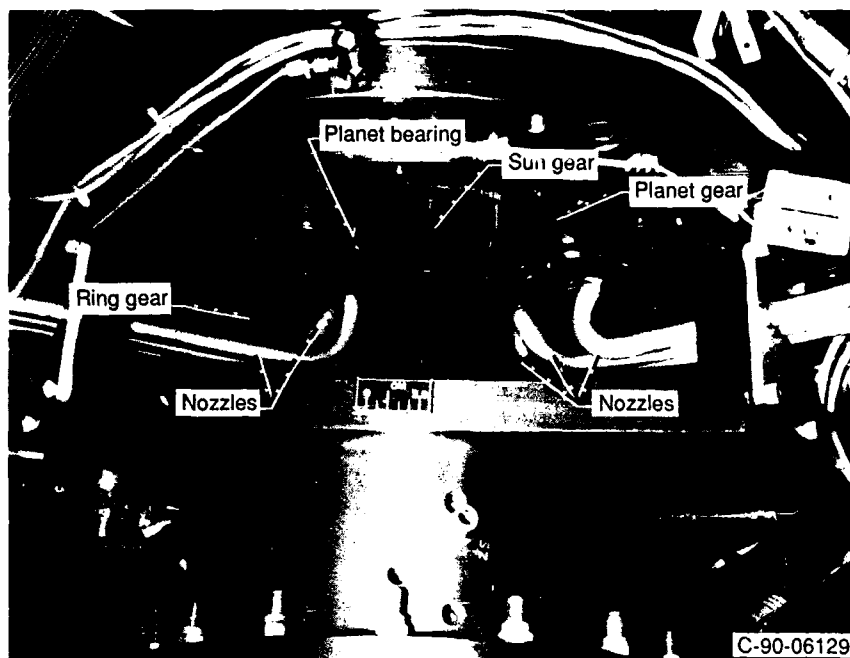


Figure 4.—Location of lubrication nozzles with respect to test rig gears and bearings.

rings. The data from these experiments were used in the present study to determine rig tare losses as a function of both temperature and input shaft speed.

Test Procedure and Data Reduction

For each test the first variable to be stabilized was the oil-inlet temperature. Once the required oil-inlet temperature was reached, the oil flow rate, the shaft rotational speed, and the load were set. The test rig was then run at these conditions for typically 10 min in order to reach steady state before data were taken. Bearing temperatures and torques were stable after typically 5 min. For each test at least five sets of data were taken, and each set of data consisted of five consecutive 2-sec scans averaged to produce one set. Thus, at least 25 scans were averaged for each test. Inspection of the data after testing showed no significant changes in the raw data between the five sets of data taken at the same conditions. The entire cycle was repeated for each test condition.

A total of 124 different tests were conducted. The variables altered during the test program were shaft rotational speed, load, lubricant flow rate, oil-inlet temperature, and lubricant type. The maximum test conditions of 100-percent sun gear speed and 100-percent sun gear total torque were 1620 rpm and 1405 N-m (12 450 in.-lbf), respectively.

So that the losses based on a given set of conditions could be measured, the torque required to drive the complete system was monitored. The torque to rotate the test planetary section, because of its losses, was assumed to be half of the torque

remaining after the rig tare losses were subtracted from the total drive motor torque. An equal split of the losses was assumed because, except for direction of rotation, the test and slave planetary sections were identical in their gear and bearing configuration, lubrication flow rate, lubricant type, and oil-inlet temperature for all tests conducted.

Operating efficiency η was computed from the following equation:

$$\eta = \frac{\left[P_{T,in} - 0.5(P_{dm} - P_{tare}) \right] \times 100}{P_{T,in}}$$

where $P_{T,in}$ is the total input power to the test planetary section. This equals the loop power on the high-speed shaft plus the drive motor power minus the input stub shaft losses. The net loss of the test and slave planetary sections equals the drive motor power minus the facility tare losses ($P_{dm} - P_{tare}$).

An uncertainty analysis (ref. 12) was performed on this equation. The accuracy of the result is a function of the test conditions and the uncertainties in the measured quantities. For this equation the worst situation is when the test rig torque is low (10 percent of full torque) and the inaccuracy of the measuring instruments is high. Two example cases (table II) show that the assumed accuracy along with the test conditions can affect the uncertainty in the calculated efficiency.

TABLE II.—RESULTS FROM UNCERTAINTY ANALYSIS

Test measurements and calculated facility losses	Test condition or calibration value		Assumed accuracy, percent	Uncertainty in efficiency calculation, percent
	N-m	in.-lbf		
Case 1: 100 percent torque; high accuracy				
High-speed shaft torque	1410	12 450	± 1.0	± 0.011
Drive motor input torque	24.5	217	± 1.2	
Facility tare loss	2.4	21.2	± 4	
Input shaft loss	.9	8	± 4	
Case 2: 10 percent torque; low accuracy				
High-speed shaft torque	165	1460	± 4	± 0.072
Drive motor input torque	5	44.2	± 10	
Facility tare loss	2.4	21.2	± 4	
Input shaft loss	.9	8	± 4	

Analytical Methods

Analysis of Bearing and Gear Mesh Loss

In order to model the efficiency of a planetary gear train, many sources of power loss must be considered. The losses from meshing gears include sliding, rolling, windage, and lubricant displacement losses. The planet bearings' losses also contribute to the total planetary system loss. The sum of these loss components was used to predict the planetary stage efficiency.

A computer program, SPHERBEAN (refs. 13 and 14), was used to predict losses from the spherical planet bearings. Input variables to the program include bearing geometry, lubricant properties, and operating speeds, loads, and temperatures. The program predicts bearing performance, including power loss.

Two computer programs, EXTERN and INTERN, were used to predict gear mesh sliding, rolling, and windage losses. These programs have been developed at the NASA Lewis Research Center. Program EXTERN models two external gears meshing; program INTERN models an internal gear meshing with an external gear. The two programs are based on the methods of references 7 and 8. The windage losses are based on a model developed from investigations of turbine wheel

windage. The rolling losses are associated with the formation of an elastohydrodynamic (EHD) film as the gear tooth surfaces roll over each other. The EHD film resists the motion of the gears and thus causes a power loss. The calculations for power loss due to sliding include a model for the coefficient of friction based on the data of reference 15.

The gear geometry data used in the analysis are shown in table I, and the lubricant properties used are shown in table III.

The analytical technique just described, which is identical to that used in reference 4, does not account for the power loss due to oil trapped by the gear teeth being displaced as the gears mesh. Reference 2, which calls this phenomenon oil trapping losses, shows that the power expended to displace the lubricant can be significant. Two different models to predict these oil displacement losses were studied in order to improve the analytical prediction of planetary system losses.

Analytical Modeling of Oil Displacement Losses

Two models for predicting the power loss due to displacing oil trapped by gear teeth were studied. The first model accounts for viscous friction effects in the flow but ignores inertia effects. The second model assumes that the fluid is frictionless

TABLE III.—LUBRICANT PROPERTIES USED FOR ANALYSIS AND CALCULATIONS

Lubricant ^a	Temperature		Thermal conductivity		Pressure viscosity coefficient		Temperature-viscosity coefficient		Kinematic viscosity		Specific gravity	Specific heat, $\frac{\text{Btu}}{\text{lbm} \cdot ^\circ\text{F}}$ or $\frac{\text{cal}}{\text{gm} \cdot ^\circ\text{C}}$
	$^\circ\text{C}$	$^\circ\text{F}$	$\frac{\text{W}}{\text{m} \cdot ^\circ\text{C}}$	$\frac{\text{Btu}}{\text{hr ft} \cdot ^\circ\text{F}}$	$\frac{1}{\text{GPa}}$	$\frac{1}{\text{psi}}$	$\frac{1}{^\circ\text{C}}$	$\frac{1}{^\circ\text{F}}$	cSt	$\frac{\text{ft}^2}{\text{sec}}$		
K (turbine engine oil)	40	104.0	0.115	0.066	11.40	7.86×10^{-5}	0.0223	0.0124	26.39	28.39×10^{-5}	0.9829	0.464
	82	179.6	.115	.066	---	---	0.0223	.0124	7.61	8.19	.9721	.495
	100	212.0	.115	.066	9.50	6.55	.0223	.0124	5.09	5.48	.9725	.507
E (formulated gear lubricant)	40	104.0	0.121	0.070	15.53	10.70×10^{-5}	0.0232	0.0129	33.91	36.50×10^{-5}	0.9322	0.680
	82	179.6	.121	.070	---	---	.0232	.0129	8.91	9.59	.9211	.730
	100	212.0	.121	.070	11.51	7.94	.0232	.0129	5.87	5.48	.9201	.767

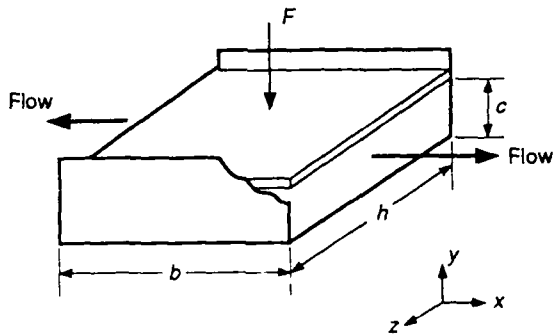
^aFrom reference 1.

Figure 5.—Oil displacement model of reference 2.

and incompressible but accounts for inertia effects. Details of the two models follow.

The first model studied was one developed by Ariura et al. (ref. 2). In their work the oil trapped between gear teeth is modeled by oil in a rectangular channel (fig. 5). A plate that just fits in the channel moves downward at some known velocity owing to a force on the plate. As the plate moves downward, oil is forced out of the channel, thereby simulating the fluid flow due to the meshing gear teeth. The flow from the channel is assumed to have the following characteristics:

(1) The fluid is an incompressible, Newtonian fluid and the viscosity of the fluid is constant everywhere.

(2) The boundary between fluid and air remains a plane.

(3) The velocity profile is not a function of the Z coordinate of figure 5.

(4) The flow is symmetric about the center of the channel length.

(5) Inertia terms in the energy equation for the fluid flow are negligible relative to viscous terms.

(6) The channel is completely filled with oil.

Under these assumptions, the work done by force F (fig. 5) as the plate moves from height c_1 to height c_2 is given by

$$W = \int_{c_1}^{c_2} F dc = \int_{c_1}^{c_2} \frac{-b^3 h \mu}{c^3} \frac{dc}{dt} dc \quad (1)$$

where

c height of channel

b length of channel

h width of channel

μ absolute viscosity of fluid

dc/dt velocity of plate

Details of the development of equation (1) are given in reference 2.

So that equation (1) could be applied to predict oil displacement losses in a gear mesh, all of the terms in the equation were selected such that the flow from the channel would represent the flow from the gear mesh. The dimensions of the channel and the velocity of the plate in the channel were chosen so that the area available for flow from the channel and the rate of change of the channel volume would equal that of the gear mesh being analyzed. Details of how equation (1) was applied to calculate the work done during one mesh cycle to displace trapped oil are given in the appendix.

A second model for calculating the work done to displace oil was developed and studied. Pechersky and Wittbrodt (ref. 16) present a method for predicting the velocity of the fluid being forced from a gear mesh. In this model the fluid is assumed to be frictionless and incompressible, and all other terms in the energy equation for the fluid flow are assumed to be negligible relative to the inertia terms. For a frictionless, incompressible fluid, the dimensionless velocity of the fluid being displaced from the gear mesh is given by (ref. 16)

$$v_r = \left(\frac{1}{Ar_p} \right) \frac{dV}{d\theta} \quad (2)$$

where

A area available for flow

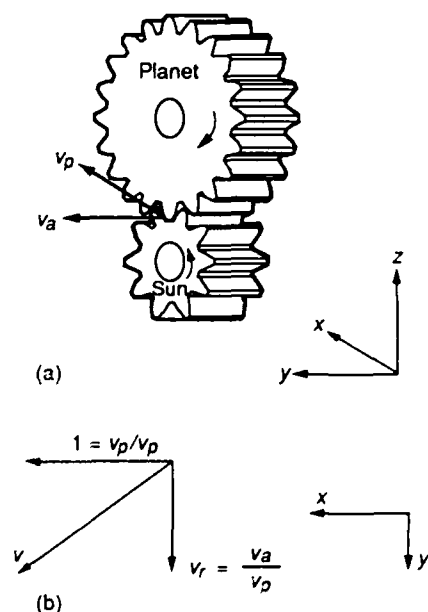
r_p pitch radius of pinion

$dV/d\theta$ rate of change of trapped volume with respect to angular position of pinion

The dimensionless velocity v_r is the ratio of the fluid velocity divided by the pitch line velocity and is relative to a control volume formed by the meshing gear teeth. In the case of a planet gear meshing with a stationary ring, the control volume is stationary and equation (2) gives the absolute dimensionless velocity. In the case of a planet gear meshing with a sun gear, the control volume is moving at the pitch line velocity of the sun gear. Therefore, the velocity of the fluid displaced from the sun-planet mesh has two components. The dimensionless velocity v_r calculated by equation (2) is one component, and the normalized pitch line velocity is the second component (fig. 6). Since these components are normal to each other, the dimensionless absolute velocity v of the fluid exiting a sun gear meshing with a planet is given by

$$v = (v_r^2 + 1)^{1/2} \quad (3)$$

Since all other terms in the energy equation for the fluid flow are assumed to be negligible relative to inertia terms,



(a) Components of fluid velocity.

(b) Velocity diagram for normalized components, where v_r is the normalized velocity calculated by equation (2) and v is the normalized resultant velocity.

Figure 6.—Velocity components of fluid displaced from sun-planet mesh, where v_p is the tangential component (sun pitch line velocity) and v_a is the axial component.

the kinetic energy of the fluid exiting the gear mesh equals the work done by the gears to displace oil. (The initial kinetic energy of the fluid was set to zero, since the oil jets were directed axially and the flow was assumed to be symmetric.) The starting point of the analysis, when oil is first displaced from the mesh, was assumed to be when the tip of the invading tooth crosses the pitch diameter of the mating gear. As the gears roll through the mesh, the oil is displaced. The ending point of the analysis is when the volume trapped by the gears is a minimum. The analysis was broken into many equal-sized steps between the starting and ending points. Over each step the amount of fluid exiting the mesh was calculated from the change in trapped volume over the step, and the velocity of the fluid at the middle of the step was calculated by using equations (2) and (3) as appropriate. The kinetic energy of the fluid exiting the gear mesh over the step can be approximated by

$$(KE)_{\text{step}} \cong \frac{1}{2} m_{\text{step}} v^2 \quad (4)$$

where

m_{step} mass of fluid exiting mesh over step

v velocity of fluid exiting mesh at middle of step

The sum of the kinetic energies calculated by using equation (4) for all steps covering the starting to the ending points of the analysis then represents the work done by the gears to displace oil over one mesh cycle.

Application of Displacement Loss Model to Planetary Stage

The two models for oil displacement loss described previously were applied to calculate the total oil displacement loss in the planetary stage being studied. In order to do this, the epicyclic motion and the lubrication method were considered. First, the displacement loss for one mesh cycle was calculated, using the previously described models, for each of four cases: a sun gear tooth invading between two planet gear teeth, a planet gear tooth invading the sun gear, a planet gear tooth invading the ring gear, and a ring gear tooth invading the planet gear.

Second, the epicyclic motion was considered. Because of the carrier motion the location of the meshing teeth with respect to the lubrication jets is constantly changing. Therefore, the amount of oil trapped by gear teeth and subsequently displaced is also constantly changing. In this study I assumed that three tooth spaces become filled with oil each time a planet gear passes a jet and that otherwise, when the planet gear is not passing a jet, no oil displacement losses occur. This assumption was used to determine the number of mesh cycles that displace oil during one rotation of the carrier. This result was combined with the calculations of work done per mesh cycle

to determine the work done by the gears in displacing oil over one rotation of the carrier. The power loss of the planetary stage due to oil displacement was then calculated by dividing the work done by the time required for one carrier rotation.

Results and Discussion

Results of Experiments

The results of the parametric study to experimentally measure the efficiency of the planetary section are shown in table IV. The two lubricants used in the parametric tests were the oils "E" and "K" from reference 2 (see table III). Lubricant E is a formulated gear lubricant (a dibasic acid ester), and lubricant K is a turbine engine oil (a mixture of 99 percent pentaerythritol ester (PE) and 1 percent dipentaerythritol ester (DPE)). The highest efficiency (99.83 percent) was measured while testing lubricant K and operating at the highest speed, the lowest load, and the lowest oil-inlet temperature tested. The lowest efficiency (98.64 percent) was measured while testing lubricant E and operating at the lowest speed, the highest load, and the highest oil-inlet temperature

tested. The efficiency measured while testing at full power ranged from 99.25 to 99.41 percent depending on the lubrication parameters.

The efficiency as a function of torque is shown in figure 7 for three speeds at the same lubrication conditions for each lubricant. For both lubricants the efficiency increased with increasing speed.

The effect of oil-inlet temperature on efficiency at 100 percent speed and at constant lubricant flow rate and pressure is shown in figure 8. For lubricant E the highest efficiency was measured at an 82 °C (180 °F) oil-inlet temperature. However, for lubricant K the lowest efficiency was measured at 82 °C (180 °F). Intuitively, one would expect the efficiency to increase as the temperature increased and the oil viscosity decreased. However, temperature-dependent properties of the oil other than viscosity can also affect the efficiency.

Another parametric effect studied was the effect of oil flow rate. The oil flow rate was changed by closing the oil flow to certain nozzles. Nozzles were closed equally for both the test and slave planetary sections. As shown in figure 9, the lubricant was supplied to each planetary section from nozzle assemblies at several positions on each side. Nozzles to each area of the planetary sections (sun-planet mesh, planet-ring mesh, and planet bearings) were fed through a separate manifold with control valves for each nozzle. Thus, specific

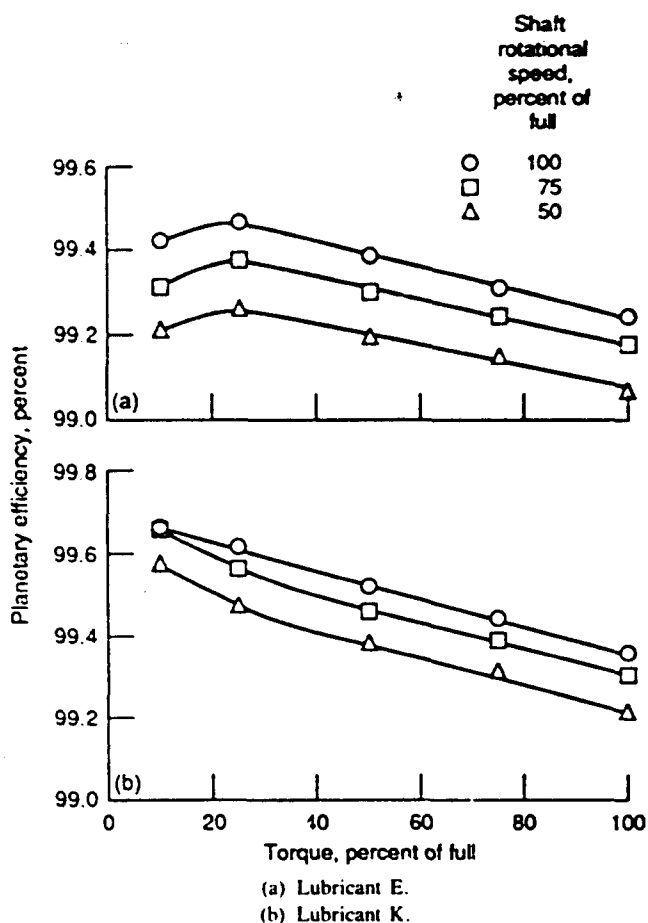


Figure 7.—Planetary efficiency as a function of torque for three speeds. Oil-inlet temperature, 99 °C (210 °F); oil flow rate per stage, 190 cm³/sec (3.0 gal/min).

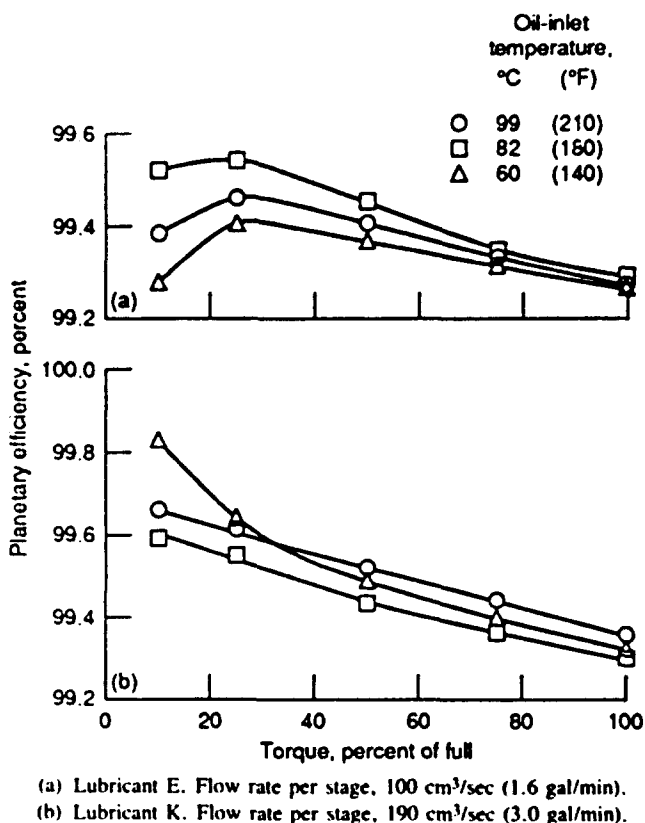


Figure 8.—Planetary efficiency as a function of torque for three oil-inlet temperatures.

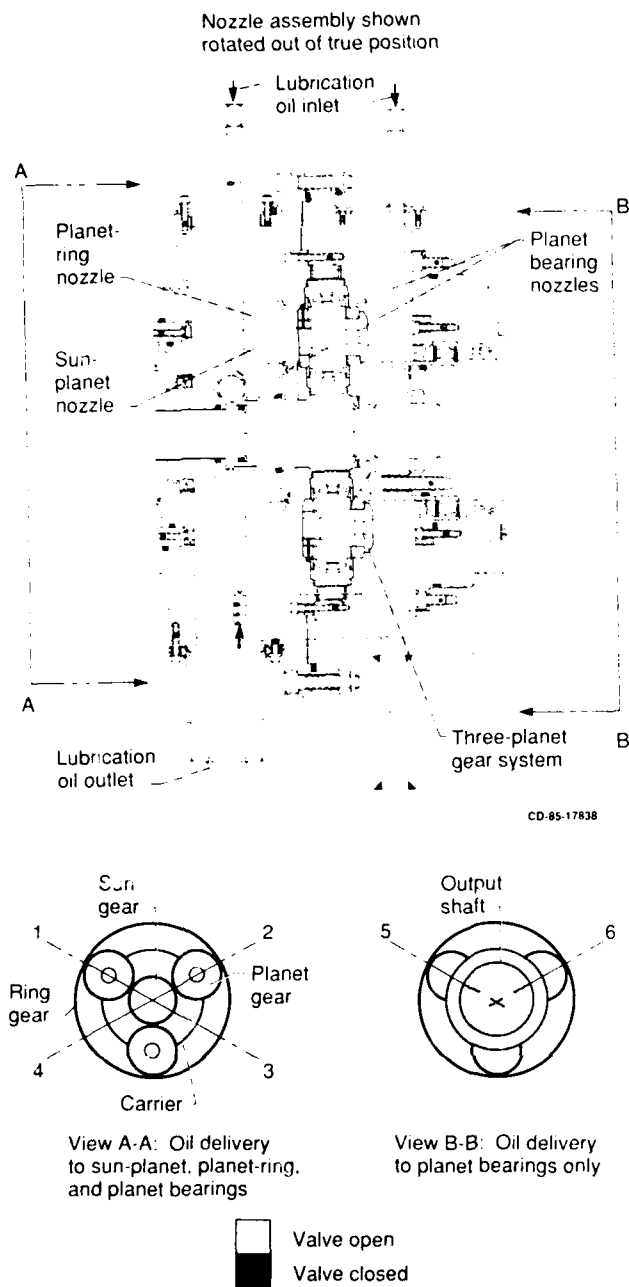


Figure 9.—Oil nozzle orientation for planetary test- and slave-section lubrication and its effect on flow rate.

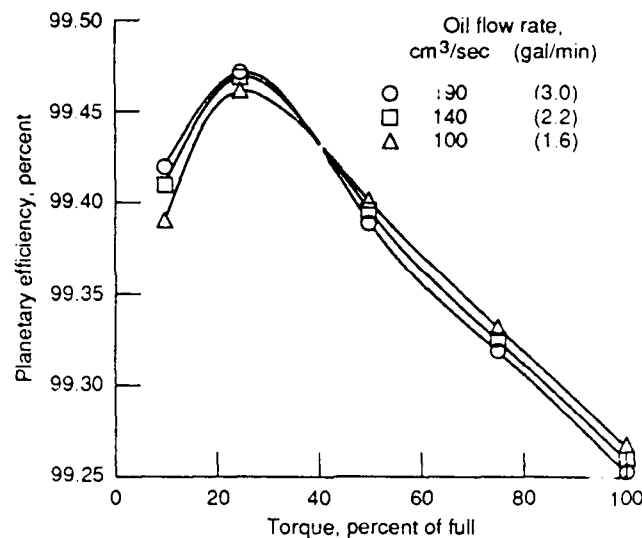


Figure 10.—Planetary efficiency as a function of torque for three oil flow rates. Lubricant E; lubricant inlet temperature, 99 °C (210 °F); shaft rotational speed, 100 percent.

total flows were obtained by opening or closing a nozzle valve as indicated in figure 9. Closing some nozzles resulted in a slightly higher flow rate per nozzle (approximately 5 percent increase in flow rate per nozzle when changing from 190 to 100 cm³/sec (3.0 to 1.6 gal/min) because of an increase in manifold pressure). Flow to each planetary area was maintained in all cases.

Figure 10 shows the effect of oil flow rate at full speed, constant temperature, and constant pressure for lubricant E. The effect of flow rate on efficiency was small. The data for lubricant K have a similar trend.

Figures 7, 8, and 10 show the effect of torque on efficiency for various conditions. In all cases the efficiency increased with decreasing torque except at extremely light torques, where zero-load losses can begin to dominate.

Most of the testing was done with a pressure to the lubricant distribution manifolds of 1240 kPa (180 psi) so that direct comparisons could be made with the data of reference 4. Since this condition does not reflect the normal operating conditions of the transmission, a number of measurements were made at a greatly reduced lubricant pressure of 210 kPa (30 psi). Comparing the results (table IV) of the measurements at different pressures but otherwise identical conditions shows that the effect of testing at high lubricant pressure is negligible.

The data in figures 7, 8, and 10 also show that the effect of lubricant flow rate was not significant relative to the effects of speed, oil temperature, and torque. For nearly all measurements made, the efficiency was higher with lubricant K than with lubricant E for the same operating conditions.

Results of Analysis

The results of the previously described analysis to calculate the power loss from the planetary stage are shown in

TABLE IV — PLANETARY STAGE EFFICIENCY BASED ON EXPERIMENTAL RESULTS
 (100 Percent speed, 1520 rpm, 100 percent torque, 140 N·m (12,450 in.-lb ft))

Oil-inlet temperature, °C	Volume flow rate, cm ³ /sec	Shaft rotational speed, percent of full	Load, percent of full	Measured planetary efficiency, %, percent	Oil-inlet temperature, °C	Volume flow rate, cm ³ /sec	Shaft rotational speed, percent of full	Load, percent of full	Measured planetary efficiency, %, percent																																																																																																																																																																																																																																																																																								
Lubricant E (pressure, 1240 kPa, 180 psi)					Lubricant K (pressure, 1240 kPa, 180 psi)																																																																																																																																																																																																																																																																																												
60	100	100	10	99.28	60	100	100	10	99.83																																																																																																																																																																																																																																																																																								
			25	99.41				50	99.36	75	99.31	100	99.25	190	15	100	98.90	190	100	10	99.83	100	99.01	100	99.13	10	99.23	25	99.38	100	50	99.32	82	100	10	99.75	75	99.25	100	99.22	10	99.22	25	99.38	100	50	99.35	190	10	99.59	75	99.29	100	99.25	82	100	100	10	99.52	82	100	100	10	99.65	25	99.44	50	99.45	75	99.34	100	99.29	190	15	100	98.79	190	100	10	99.66	100	98.95	100	99.13	10	99.47	25	99.48	100	50	99.56	99	100	10	99.66	75	99.29	100	99.22	10	99.49	25	99.51	99	100	100	10	99.39	99	100	100	10	99.66	25	99.46	50	99.40	75	99.33	100	99.26	140	100	10	99.41	140	100	10	99.66	25	99.47	50	99.40	75	99.32	100	99.26	190	15	75	98.66	190	15	75	99.00	100	98.64	100	98.91	100	98.84	10	99.21	100	25	99.26	100	25	99.15	50	99.19	75	99.15	100	99.07	10	99.32	99	100	100	10	99.39	99	100	100	10	99.61	25	99.25	50	99.39	75	99.32	100	99.25																																																																																																								
			50	99.36				75	99.31	100	99.25	190	15			100	98.90			190	100	10	99.83	100	99.01	100	99.13	10	99.23		25	99.38			100	50	99.32	82	100	10	99.75	75	99.25	100		99.22	10		99.22	25	99.38	100	50	99.35				190	10				99.59	75	99.29	100	99.25	82	100	100	10	99.52			82	100			100	10	99.65	25	99.44	50	99.45	75	99.34	100		99.29	190			15	100	98.79	190	100	10	99.66	100	98.95	100				99.13	10				99.47	25	99.48	100	50	99.56	99	100	10	99.66			75	99.29			100	99.22	10	99.49	25	99.51	99	100	100	10			99.39	99			100	100	10	99.66	25	99.46	50	99.40	75	99.33		100	99.26		140	100	10	99.41	140	100	10	99.66	25	99.47				50	99.40				75	99.32	100	99.26	190	15	75	98.66	190	15	75	99.00	100	98.64	100	98.91	100	98.84	10	99.21	100	25	99.26	100	25	99.15	50	99.19	75	99.15	100	99.07	10	99.32	99	100	100	10	99.39	99	100	100	10	99.61	25	99.25	50	99.39	75	99.32	100	99.25																																																														
			75	99.31				100	99.25	190	15					100	98.90					190	100	10	99.83	100	99.01	100	99.13		10	99.23				25	99.38			100	50	99.32	82	100		10	99.75		75	99.25	100		99.22	10					99.22				25	99.38	100	50	99.35				190	10								99.59	75	99.29	100	99.25	82	100	100	10		99.52					82	100			100	10	99.65	25	99.44				50	99.45				75	99.34	100		99.29	190			15	100			98.79	190			100	10	99.66	100	98.95	100				99.13			10						99.47	25	99.48	100	50	99.56	99	100		10	99.66				75	99.29			100	99.22	10	99.49				25	99.51				99	100	100	10			99.39	99			100	100	10	99.66	25	99.46	50	99.40	75	99.33		100	99.26		140	100	10	99.41	140	100	10	99.66	25	99.47				50	99.40				75	99.32	100	99.26	190	15	75	98.66	190	15	75	99.00	100	98.64	100	98.91	100	98.84	10	99.21	100	25	99.26	100	25	99.15	50	99.19	75	99.15	100	99.07	10	99.32	99	100	100	10	99.39	99	100	100	10	99.61	25	99.25	50	99.39	75	99.32	100	99.25																				
			100	99.25																																																																																																																																																																																																																																																																																													
	190	15	100	98.90		190	100	10	99.83																																																																																																																																																																																																																																																																																								
			100	99.01				100	99.13						10	99.23	25		99.38					100	50	99.32	82	100	10	99.75	75	99.25		100		99.22	10				99.22	25			99.38	100	50	99.35	190	10	99.59	75	99.29	100		99.25	82	100	100		10	99.52	82	100	100	10	99.65				25	99.44		50				99.45		75	99.34	100	99.29	190				15	100	98.79		190	100							10	99.66	100	98.95		100	99.13	10	99.47		25	99.48	100	50	99.56		99					100		10	99.66			75		99.29	100	99.22	10	99.49				25		99.51	99			100			100	10	99.39		99	100				100	10				99.66	25			99.46	50	99.40	75	99.33	100	99.26	140	100	10	99.41	140				100			10						99.66	25	99.47	50	99.40	75	99.32	100		99.26	190				15	75			98.66	190	15	75				99.00	100				98.64	100	98.91	100			98.84	10			99.21	100	25	99.26	100	25	99.15	50	99.19	75		99.15	100		99.07	10	99.32	99	100	100	10	99.39	99	100				100	10				99.61	25	99.25	50	99.39	75	99.32	100	99.25																					
			100	99.13				10	99.23				25		99.38	100	50		99.32		82				100	10			99.75	75	99.25	100		99.22	10	99.22	25		99.38		100	50			99.35		190	10		99.59	75	99.29	100	99.25		82					100	100				10	99.52		82	100	100	10		99.65		25		99.44	50	99.45	75	99.34	100						99.29	190				15				100		98.79	190	100	10		99.66	100	98.95	100		99.13	10		99.47	25	99.48			100	50				99.56	99			100		10	99.66	75	99.29	100		99.22	10	99.49		25					99.51	99		100	100								10			99.39	99	100		100	10	99.66	25	99.46	50	99.40	75			99.33	100							99.26	140			100			10	99.41	140	100	10	99.66	25	99.47		50						99.40			75			99.32	100	99.26	190	15	75	98.66	190	15	75	99.00	100	98.64			100	98.91			100		98.84	10		99.21	100	25	99.26	100		25	99.15		50	99.19	75				99.15	100							99.07				10	99.32	99	100	100	10	99.39	99	100	100	10	99.61	25	99.25	50	99.39	75	99.32	100	99.25										
			10	99.23				25	99.38		100		50		99.32		82		100				10			99.75			75	99.25	100	99.22		10	99.22	25	99.38		100	50		99.35		190	10			99.59		75	99.29	100	99.25	82												100	100					10		99.52		82		100	100	10	99.65	25	99.44			50	99.45		75							99.34		100	99.29	190			15		100	98.79	190	100		10	99.66		100	98.95	100				99.13	10			99.47					25	99.48	100	50	99.56	99		100	10	99.66		75					99.29					100			99.22	10			99.49			25					99.51	99	100	100	10	99.39	99			100	100			10	99.66			25					99.46	50	99.40	75			99.33	100	99.26	140		100				10		99.41		140	100			10	99.66	25			99.47	50			99.40	75	99.32	100		99.26	190	15		75	98.66		190	15		75		99.00	100			98.64	100		98.91	100	98.84				10	99.21			100	25	99.26		100	25	99.15	50	99.19	75				99.15	100				99.07	10	99.32	99	100	100	10	99.39	99	100	100	10	99.61	25	99.25	50	99.39	75	99.32	100
			25	99.38																																																																																																																																																																																																																																																																																													
		100	50	99.32			82	100	10				99.75																																																																																																																																																																																																																																																																																				
			75	99.25					100				99.22		10								99.22	25		99.38		100	50	99.35	190	10	99.59	75	99.29	100	99.25	82	100	100	10	99.52	82	100	100	10	99.65	25	99.44	50	99.45	75	99.34					100	99.29					190	15							100	98.79	190			100			10	99.66	100	98.95			100	99.13	10	99.47				25			99.48		100	50						99.56	99				100	10	99.66	75	99.29	100	99.22			10	99.49	25		99.51					99	100		100	10				99.39	99		100				100	10		99.66			25		99.46	50	99.40	75	99.33	100	99.26		140					100				10	99.41			140					100	10	99.66		25					99.47	50	99.40	75			99.32	100	99.26							190	15	75					98.66	190	15	75			99.00	100			98.64	100	98.91	100		98.84				10	99.21					100		25	99.26			100	25		99.15	50	99.19	75	99.15	100	99.07	10	99.32	99		100	100	10		99.39	99	100	100	10				99.61	25				99.25	50	99.39				75	99.32				100	99.25							
			100	99.22					10				99.22		25	99.38							100	50	99.35	190			10	99.59		75	99.29	100	99.25	82	100				100	10				99.52	82	100	100	10	99.65	25	99.44					50	99.45		75	99.34								100	99.29	190	15							100	98.79	190	100			10	99.66	100	98.95		100		99.13	10		99.47	25		99.48			100			50						99.56	99	100	10	99.66	75		99.29	100	99.22	10		99.49	25			99.51					99				100								100		10	99.39	99	100		100	10	99.66	25	99.46	50	99.40				75		99.33					100	99.26									140	100		10				99.41	140	100	10	99.66		25	99.47	50	99.40		75			99.32				100					99.26			190		15	75	98.66		190	15	75	99.00	100		98.64				100	98.91							100	98.84				10		99.21	100	25	99.26	100	25	99.15	50	99.19					75		99.15				100	99.07	10	99.32	99	100	100	10	99.39	99	100	100				10	99.61				25	99.25	50	99.39	75	99.32	100	99.25	
			10	99.22					25		99.38		100		50	99.35			190					10	99.59				75	99.29		100	99.25	82	100							100				10				99.52	82	100	100					10	99.65		25	99.44				50	99.45			75	99.34							100	99.29	190	15					100	98.79	190	100		10		99.66	100		98.95	100		99.13				10		99.47			25			99.48			100	50	99.56	99	100	10	99.66	75		99.29	100	99.22		10			99.49			25		99.51											99	100					100	10	99.39	99	100	100				10		99.66			25	99.46	50	99.40				75	99.33							100				99.26			140	100		10	99.41	140	100		10	99.66		25				99.47			50		99.40						75	99.32				100	99.26	190		15		75		98.66	190			15				75	99.00		100		98.64	100	98.91		100	98.84		10	99.21	100	25					99.26		100				25	99.15	50	99.19				75	99.15				100	99.07	10	99.32	99	100	100	10	99.39	99	100	100	10	99.61	25	99.25	50
			25	99.38																																																																																																																																																																																																																																																																																													
		100	50	99.35				190	10		99.59																																																																																																																																																																																																																																																																																						
			75	99.29					100	99.25	82	100	100	10	99.52	82	100	100	10	99.65	25	99.44	50	99.45	75	99.34	100	99.29	190	15	100	98.79	190						100	10				99.66	100	98.95				100					99.13			10	99.47	25	99.48	100			50	99.56	99			100	10						99.66	75	99.29					100		99.22	10				99.49	25	99.51	99		100	100	10	99.39				99		100	100		10		99.66	25				99.46	50			99.40	75	99.33		100	99.26	140		100		10	99.41	140		100		10			99.66	25			99.47	50										99.40	75							99.32		100	99.26		190	15	75	98.66				190	15			75				99.00				100						98.64	100				98.91	100		98.84			10	99.21			100		25		99.26				100	25				99.15	50					99.19		75		99.15			100			99.07	10		99.32		99	100	100		10	99.39		99	100		100	10		99.61	25	99.25			50	99.39	75	99.32	100	99.25																										
			100	99.25					82	100				100	10				99.52	82	100	100	10	99.65	25	99.44	50	99.45			75	99.34					100			99.29	190			15	100	98.79		190	100	10					99.66			100	98.95	100	99.13				10	99.47		25			99.48		100		50		99.56	99	100				10	99.66		75	99.29			100	99.22	10	99.49					25	99.51		99	100						100		10	99.39	99	100		100	10			99.66	25	99.46		50	99.40					75	99.33					100	99.26		140	100			10	99.41	140					100		10		99.66	25							99.47		50	99.40				75	99.32								100		99.26	190	15			75	98.66		190				15	75				99.00	100		98.64			100	98.91					100		98.84			10		99.21			100	25	99.26					100		25		99.15			50		99.19	75	99.15	100	99.07						10	99.32						99		100	100	10			99.39	99	100	100	10	99.61	25	99.25	50	99.39	75	99.32	100	99.25																		
82	100	100	10	99.52	82	100	100	10							99.65																																																																																																																																																																																																																																																																																		
			25	99.44				50							99.45				75				99.34	100	99.29	190	15	100			98.79	190			100		10			99.66		100			98.95	100				99.13		10	99.47		25			99.48	100	50	99.56				99	100		10			99.66				75		99.29				100		99.22	10	99.49	25	99.51		99	100	100	10	99.39		99			100	100	10							99.66			25	99.46			50		99.40	75	99.33	100	99.26	140		100	10					99.41	140					100	10						99.66	25				99.47				50	99.40	75	99.32		100	99.26				190		15	75				98.66	190								15		75					99.00	100				98.64			100		98.91		100	98.84		10			99.21	100					25		99.26			100		25				99.15	50		99.19	75			99.15	100		99.07		10	99.32		99	100	100	10	99.39						99	100							100			10	99.61		25				99.25	50	99.39	75	99.32	100	99.25																					
			50	99.45				75							99.34				100				99.29	190	15			100			98.79						190			100		10			99.66	100				98.95		100	99.13		10			99.47		25	99.48							100			50				99.56		99				100		10	99.66	75	99.29	100					99.22	10							99.49							25			99.51	99			100		100	10	99.39	99	100				100					10							99.66						25	99.46				50				99.40	75	99.33	100		99.26	140							100				10											99.41					140	100				10			99.66		25		99.47	50		99.40			75						99.32		100					99.26				190	15		75	98.66			190	15		75		99.00	100					98.64	100																	98.91	100		98.84				10	99.21	100	25	99.26	100	25	99.15	50	99.19	75	99.15	100	99.07	10	99.32	99	100	100	10	99.39	99	100	100	10	99.61	25	99.25
			75	99.34				100				99.29	190		15		100	98.79	190				100					10		99.66	100								98.95			100			99.13	10				99.47		25	99.48		100		50	99.56		99	100	10	99.66	75			99.29			100	99.22			10	99.49								25	99.51	99	100	100					10	99.39			99	100			100					10	99.66	25			99.46							50	99.40				75				99.33	100		99.26				140			100						10	99.41				140				100	10	99.66	25		99.47											50	99.40						75					99.32										100			99.26		190		15	75	98.66	190			15					75	99.00		100					98.64							100	98.91						100		98.84	10	99.21				100	25	99.26	100	25	99.15					50	99.19		75					99.15	100		99.07				10	99.32		99	100		100	10	99.39	99	100	100	10	99.61	25	99.25				50	99.39				75	99.32	100	99.25
			100	99.29				190		15		100		98.79			190	100			10	99.66						100		98.95	100								99.13			10		99.47	25	99.48			100	50		99.56	99			100	10	99.66				75	99.29	100			99.22		10	99.49	25	99.51	99	100	100			10	99.39			99	100	100								10	99.66									25			99.46	50	99.40	75		99.33			100		99.26		140	100				10				99.41	140		100										10			99.66	25						99.47			50	99.40	75		99.32		100				99.26					190	15						75					98.66		190								15		75	99.00					100	98.64									100	98.91		100		98.84			10	99.21						100	25						99.26		100	25	99.15					50	99.19		75	99.15	100			99.07	10	99.32		99	100		100	10	99.39	99		100	100	10	99.61	25	99.25						50	99.39				75	99.32	100	99.25												
	190	15	100	98.79		190	100					10		99.66																																																																																																																																																																																																																																																																																			
			100	98.95								100		99.13							10	99.47					25	99.48		100	50				99.56				99			100		10	99.66	75				99.29		100		99.22			10	99.49	25			99.51	99	100	100	10	99.39		99	100	100	10				99.66		25	99.46	50								99.40		75	99.33	100	99.26					140	100			10			99.41	140	100	10		99.66			25		99.47							50	99.40			75									99.32				100			99.26	190						15			75	98.66	190		15		75				99.00	100											98.64			100		98.91												100	98.84					10	99.21		100				25			99.26	100		25		99.15			50	99.19							75	99.15					100	99.07		10	99.32	99	100	100		10	99.39		99	100	100	10	99.61	25	99.25	50	99.39			75		99.32	100		99.25																																
			100	99.13								10		99.47							25	99.48			100		50	99.56			99				100					10				99.66	75	99.29				100		99.22		10			99.49	25	99.51			99				100	100	10				99.39				99	100	100	10	99.66	25							99.46		50	99.40	75	99.33									100			99.26			140		100			10	99.41	140	100				10		99.66	25	99.47		50									99.40				75			99.32										100	99.26					190				15	75	98.66										190			15		75						99.00						100	98.64					100	98.91						100			98.84			10		99.21			100	25				99.26			100	25			99.15		50	99.19		75	99.15					100	99.07					10	99.32	99	100	100	10			99.39		99	100		100			10	99.61	25	99.25						50	99.39				75	99.32	100	99.25												
			10	99.47								25		99.48	100						50	99.56	99				100	10	99.66				75					99.29		100			99.22	10	99.49	25				99.51		99		100	100		10	99.39	99	100	100							10				99.66							25	99.46	50					99.40	75	99.33		100	99.26	140	100				10			99.41		140		100	10				99.66				25	99.47						50		99.40	75	99.32		100									99.26	190			15			75									98.66	190	15										75	99.00							100				98.64				100						98.91						100	98.84				10	99.21	100			25	99.26		100		25	99.15		50	99.19		75		99.15		100				99.07				10			99.32		99	100		100	10					99.39	99					100	100				10			99.61								25	99.25	50	99.39		75	99.32		100	99.25																				
			25	99.48																																																																																																																																																																																																																																																																																													
		100	50	99.56			99			100		10		99.66																																																																																																																																																																																																																																																																																			
			75	99.29								100		99.22				10			99.49	25				99.51		99	100	100		10	99.39	99		100		100	10	99.66	25	99.46	50	99.40	75	99.33	100	99.26	140	100	10		99.41			140	100	10						99.66	25			99.47		50	99.40	75		99.32	100				99.26	190	15		75	98.66		190	15	75		99.00	100						98.64		100	98.91					100		98.84		10				99.21	100				25		99.26		100	25	99.15		50			99.19					75	99.15						100	99.07							10		99.32					99							100	100				10			99.39				99	100			100			10	99.61		25				99.25	50	99.39	75			99.32	100	99.25																																																																																												
			100	99.22								10		99.49				25			99.51	99		100	100	10					99.39	99	100		100		10		99.66	25	99.46	50	99.40	75	99.33	100	99.26	140			100		10					99.41						140	100	10	99.66	25		99.47	50	99.40		75	99.32		100	99.26	190				15	75				98.66		190	15						75		99.00	100					98.64		100		98.91	100			98.84			10		99.21		100			25	99.26		100			25					99.15	50						99.19	75							99.15		100											99.07						10			99.32						99					100	100		10				99.39	99	100	100			10	99.61	25				99.25	50	99.39		75	99.32	100		99.25																																																																																
			10	99.49							25	99.51	99	100	100	10		99.39	99		100		100			10	99.66				25						99.46		50	99.40	75	99.33	100	99.26	140	100	10						99.41	140	100			10		99.66	25					99.47	50	99.40		75	99.32	100		99.26	190		15	75						98.66				190					15				75		99.00	100				98.64	100		98.91		100	98.84			10			99.21		100					25	99.26					100					25	99.15				50	99.19	75	99.15							100	99.07	10		99.32						99			100				100		10			99.39	99	100												100				10						99.61	25	99.25				50	99.39	75		99.32	100	99.25																																																																																		
			25	99.51																																																																																																																																																																																																																																																																																													
99	100	100	10	99.39	99	100	100	10	99.66																																																																																																																																																																																																																																																																																								
			25	99.46				50	99.40	75	99.33	100				99.26	140	100		10						99.41	140		100	10	99.66					25	99.47	50	99.40	75	99.32	100	99.26	190			15			75			98.66				190	15		75	99.00					100	98.64	100		98.91	100	98.84		10				99.21			100			25			99.26										100		25	99.15				50	99.19		75		99.15	100			99.07			10							99.32	99										100	100				10	99.39	99	100			100				10	99.61	25		99.25			50				99.39	75		99.32	100	99.25																																																																																																																												
			50	99.40				75	99.33	100	99.26	140				100				10				99.41	140	100				10	99.66		25		99.47	50	99.40	75	99.32	100	99.26	190	15							75	98.66		190							15	75				99.00	100	98.64	100		98.91	100	98.84		10				99.21					100	25			99.26				100								25	99.15				50	99.19		75		99.15	100			99.07			10							99.32																99	100									100	10	99.39		99			100				100	10		99.61	25	99.25			50	99.39	75	99.32				100	99.25																																																																																																																	
			75	99.33				100	99.26	140	100			10	99.41					140	100		10	99.66						25	99.47		50		99.40	75	99.32	100	99.26	190	15					75				98.66	190				15						75				99.00	100	98.64	100		98.91	100	98.84		10			99.21	100						25			99.26						100						25	99.15				50	99.19		75		99.15	100			99.07			10							99.32		99			100			100						10													99.39	99								100		100	10	99.61	25	99.25	50		99.39	75	99.32	100	99.25																																																																																																																					
			100	99.26				140	100					10	99.41								140	100						10	99.66		25		99.47	50	99.40	75	99.32							100				99.26											190				15	75	98.66	190		15	75	99.00		100			98.64							100			98.91												100	98.84				10	99.21		100		25	99.26			100			25							99.15									50					99.19	75						99.15				100		99.07												10	99.32	99	100	100	10	99.39	99	100	100	10	99.61		25	99.25	50	99.39	75	99.32	100	99.25																																																																																																											
	140	100	10	99.41		140	100							10	99.66																																																																																																																																																																																																																																																																																		
			25	99.47										50	99.40			75											99.32	100	99.26		190		15	75	98.66	190	15							75	99.00			100								98.64								100	98.91				100	98.84		10			99.21							100			25												99.26	100				25	99.15				50	99.19				75		99.15					100	99.07	10	99.32						99		100		100	10		99.39	99			100	100	10	99.61	25	99.25		50		99.39				75	99.32							100	99.25																																																																																																																														
			50	99.40										75	99.32	100		99.26								190			15	75	98.66					190	15						75			99.00	100			98.64								100		98.91						100	98.84				10	99.21		100			25										99.26												100					25	99.15				50	99.19				75		99.15				100	99.07	10	99.32	99		100									100		10		99.39	99			100	100	10	99.61		25	99.25	50			99.39	75	99.32	100	99.25																																																																																																																																				
			75	99.32							100			99.26	190	15		75			98.66									190	15										75		99.00			100	98.64			100					98.91			100		98.84						10	99.21				100	25					99.26										100							25									99.15	50	99.19				75	99.15				100		99.07		10		99.32	99	100	100		10			99.39	99		100		100			10	99.61		25						99.25	50	99.39	75	99.32	100	99.25																																																																																																																																										
			100	99.26					190		15			75				98.66			190			15																	75		99.00			100	98.64			100					98.91			100		98.84					10	99.21	100			25		99.26					100																	25							99.15		50	99.19	75				99.15	100		99.07		10		99.32	99	100		100					10		99.39	99								100	100		10						99.61	25	99.25	50	99.39	75	99.32	100	99.25																																																																																																																																								
		190	15	75			98.66							190				15																							75		99.00																																																																																																																																																																																																																																																						
				100			98.64																												100				98.91		100		98.84			10	99.21			100					25			99.26		100					25	99.15				50		99.19								75	99.15					100			99.07					10	99.32		99	100			100		10	99.39	99	100			100	10		99.61		25		99.25									50		99.39			75		99.32		100				99.25																																																																																																																																																							
				100			98.91																						100						98.84		10		99.21		100		25			99.26	100								25			99.15							50	99.19				75		99.15							100	99.07	10		99.32			99			100	100	10			99.39	99								100	100				10		99.61	25	99.25		50	99.39	75			99.32					100	99.25																																																																																																																																																																				
				100			98.84									10													99.21		100				25		99.26		100				25			99.15									50			99.19							75	99.15				100		99.07			10			99.32	99	100	100		10		99.39			99			100	100	10	99.61		25						99.25						50		99.39	75	99.32		100	99.25																																																																																																																																																																														
				10			99.21				100					25								99.26					100						25		99.15						50			99.19									75			99.15							100	99.07				10		99.32	99		100			100				10	99.39		99								100	100		10						99.61					25	99.25		50	99.39	75	99.32	100	99.25																																																																																																																																																																														
			100	25			99.26									100		25						99.15																																																																																																																																																																																																																																																																									
				50			99.19											75						99.15											100		99.07						10	99.32		99			100						100	10	99.39	99					100		100	10			99.61	25		99.25										50	99.39	75												99.32	100	99.25																																																																																																																																																																																															
				75			99.15											100						99.07											10		99.32					99	100	100				10					99.39			99	100					100		10		99.61			25	99.25		50		99.39		75						99.32	100	99.25																																																																																																																																																																																																													
				100			99.07											10						99.32											99		100			100					10			99.39			99	100	100	10					99.61					25		99.25			50	99.39	75	99.32		100		99.25																																																																																																																																																																																																																					
				10			99.32											99						100																					100			10						99.39					99		100			100		10	99.61	25	99.25	50	99.39	75	99.32	100	99.25																																																																																																																																																																																																																						
				99			100																																									100						10												99.39	99	100	100	10	99.61																																																																																																																																																																																																																										
																	25										99.25	50					99.39	75				99.32								100			99.25																																																																																																																																																																																																																																																
												50					99.39					75			99.32	100	99.25																																																																																																																																																																																																																																																																						
										75		99.32	100		99.25																																																																																																																																																																																																																																																																																		
								100	99.25																																																																																																																																																																																																																																																																																								

table V. The sum of the losses calculated by using the programs SPHERBEAN (bearing losses), EXTERN (sun-planet mesh losses), and INTERN (planet-ring mesh losses) and the appropriate oil displacement model is the total loss for the planetary. For all conditions analyzed the oil displacement losses calculated with model II (inertial effects model) are much greater than those calculated with model I (viscous effects model)(table V). Reference 2 includes experimental evidence that model I predicts oil displacement losses fairly well for a highly viscous lubricant in the 280-cSt range. For the planetary system studied here the oil viscosity was in the range 5 to 20 cSt, and the viscous effects in the gear mesh no longer influenced the oil displacement losses. Therefore, oil displacement model II was chosen as the appropriate model. The results of the analysis were summed to yield the total planetary loss, and then the planetary efficiencies were calculated. The planetary efficiencies predicted by the analysis are shown in table VI.

The impact of including oil displacement losses in the analysis to predict efficiency is shown in figure 11, where analytical predictions of efficiency both with and without oil displacement losses included are compared with the experimental results. In the case of lubricant E at a 60 °C (140 °F) oil-inlet temperature, adding oil displacement losses to the analysis improved the correlation between the predicted and the experimentally measured efficiencies. In the case of lubricant K at a 99 °C (210 °F) oil-inlet temperature, adding oil displacement losses to the analysis also improved the correlation but not as significantly.

The proposed model for oil displacement losses does not fully explain the differences between the analytical and experimental results of this study nor the differences in the data of reference 4.

TABLE V.—ANALYTICALLY PREDICTED POWER LOSS

Operating conditions			Power losses per planet, W				
Oil-inlet temperature, °C	Shaft rotational speed, percent of full	Load, percent of full	Sun gear mesh losses	Ring gear mesh losses	Bearing losses	Displacement losses	
						Viscous model	Inertia model
Lubricant E							
60	30	100	85.98	25.16	31.32	0.42	1.81
	60	100	185.46	52.24	72.63	.84	7.23
	80	100	254.14	71.06	93.21	1.15	12.68
	100	30	21.92	7.76	25.50	1.40	20.13
	60		123.79	38.38	68.83		
	80		219.91	63.60	97.39		
	100		324.00	90.09	119.39	↓	↓
99	10	100	24.91	7.70	10.44	0.02	0.20
	30		46.31	17.50	37.06	.07	1.81
	60		108.43	37.47	90.61	.15	7.23
	80		153.32	51.57	111.63	.19	12.68
	100	10	3.13	.71	9.55	.24	20.13
	30		6.86	2.14	28.47		
	60		47.35	20.35	63.16		
	80		112.97	41.45	94.48		
	100		200.22	65.94	143.03	↓	↓
Lubricant K							
60	100	10	5.59	1.19	14.91	1.09	20.88
		30	12.90	1.82	47.46		
		60	55.48	11.71	98.36		
		80	116.62	28.33	142.95		
		100	201.04	50.60	206.71	↓	↓
99	100	10	2.76	0.63	17.15	0.21	20.88
		30	5.22	1.09	39.75		
		60	15.81	2.97	84.78		
		80	34.00	8.75	130.05		
		100	67.41	20.96	192.47	↓	↓

TABLE VI.—ANALYTICALLY PREDICTED PLANETARY EFFICIENCY

Oil-inlet temperature, °C	Shaft rotational speed, percent of full	Load, percent of full	Planetary efficiency, percent
Lubricant E			
60	30	100	99.40
	60	100	99.33
	80	100	99.32
	100	30	99.68
		60	99.47
		80	99.37
		100	99.30
99	10	100	99.46
	30		99.57
	60		99.51
	80		99.48
	100	10	99.58
		30	99.76
		60	99.68
		80	99.58
		100	99.46
Lubricant K			
60	100	10	99.46
		30	99.65
		60	99.61
		80	99.51
		100	99.40
99	100	10	99.48
		30	99.72
		60	99.74
		80	99.70
		100	99.62

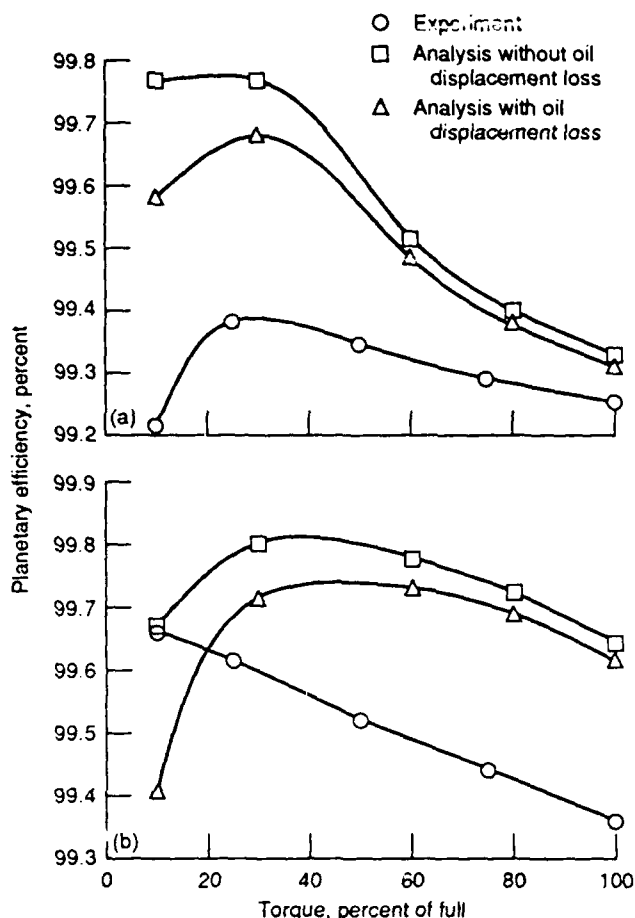


Figure 11.—Comparison of experiment with analysis (planetary efficiency versus torque).

Comparison of Analysis and Experiment

The analytical and experimental trends of planetary efficiency at varying torques for both lubricants are shown in figure 11. The trends are similar. The data shown in figure 11 are representative of results at other operating conditions. In general, the analysis predicted higher efficiencies than were measured. Also, both analysis and experiments indicated that efficiencies were greater with lubricant K than with lubricant E, and the correlation between experimental and analytical results was best at the lowest oil-inlet temperature studied (60 °C; 140 °F).

Predicted and measured efficiency results at 100 percent torque for different shaft rotational speeds are shown in figure 12. The experimental results show efficiency sharply decreasing with decreasing speed, but the analysis predicts a mild increase in efficiency with decreasing speed. The correlation between experimental and analytical results was better at the lower oil-inlet temperature.

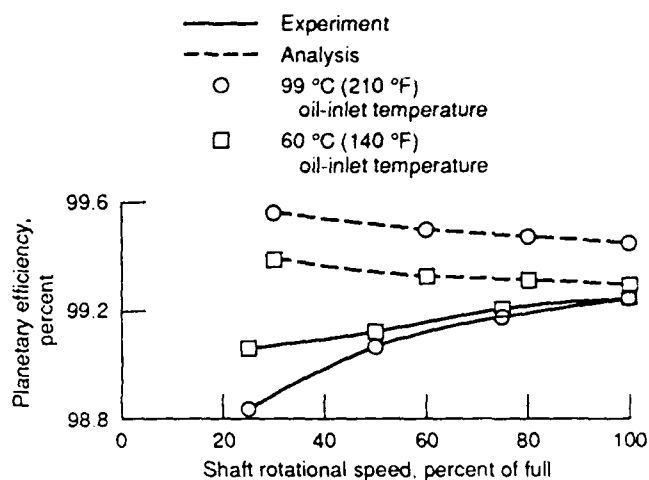


Figure 12.—Comparison of experiment with analysis (planetary efficiency versus shaft rotational speed). Lubricant E; torque, 100 percent; oil flow rate per stage, 190 cm³/sec (3.0 gal/min).

Comparison With Results of Other Studies

The results found experimentally and analytically in the study are compared here with those found by other investigators.

Comparison with reference 4.—Reference 4 reports the results of a study on the performance of a planetary stage from an Army OH-58 helicopter transmission that contained four planets and used double-row cylindrical planet bearings. The planetary stage of the present study is also from an OH-58 helicopter transmission but contains three planets and uses a

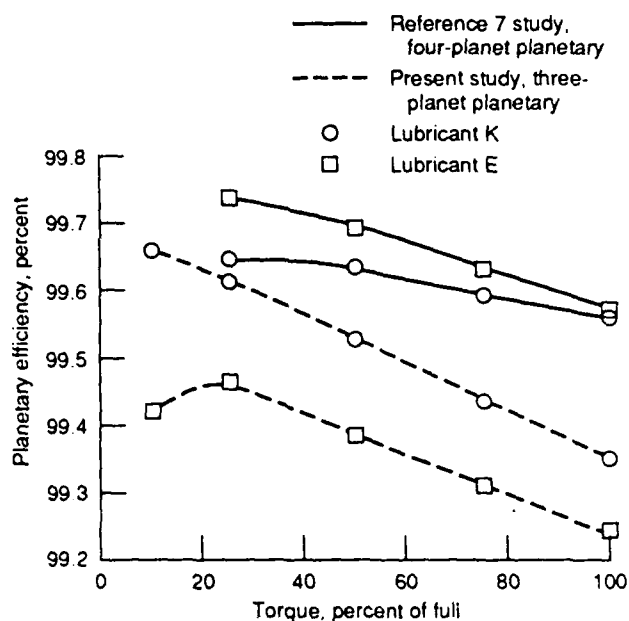
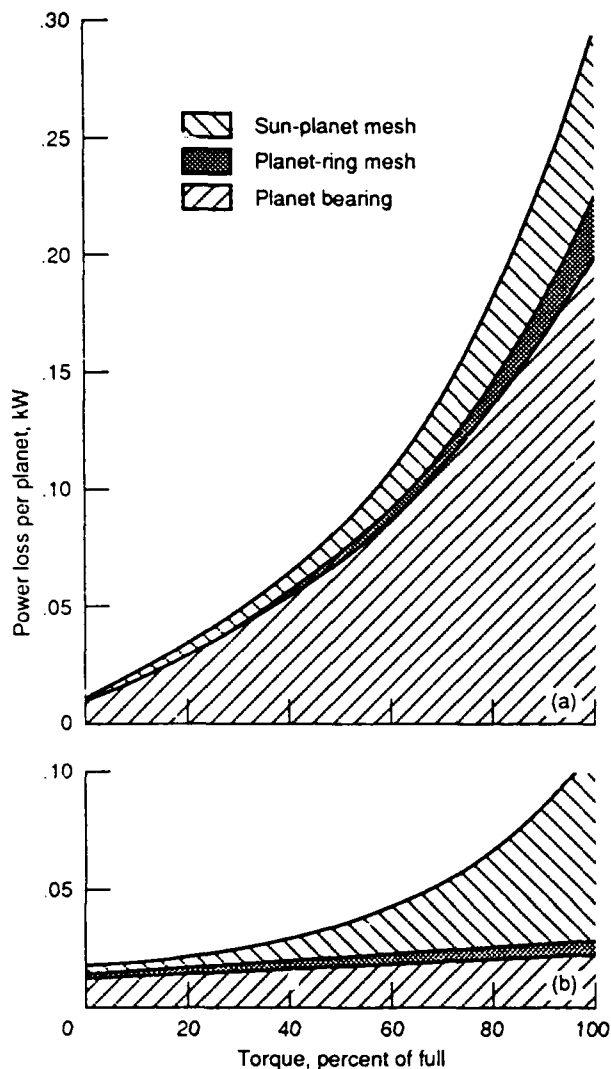


Figure 13.—Comparison of two planetary stages (planetary efficiency versus input torque). Oil-inlet temperature, 99 °C (210 °F); shaft rotational speed 100 percent; oil flow rate per stage, 190 cm³/sec (3.0 gal/min).



(a) Planetary stage with spherical bearings (present study)
(b) Planetary stage with cylindrical bearings (reference 7 study).

Figure 14.—Breakdown of analytically predicted power loss for two designs.

double row of spherical planet bearings. The gears used in the two planetary stages are the same design.

The efficiency measurements for the two planetary stages are shown in figure 13 for lubricants E and K. The figure shows that although the efficiency of the four-planet planetary was greater for lubricant E, the efficiency of the three-planet planetary was greater for lubricant K.

Also, the data indicate that the four-planet planetary stage was much more efficient than the three-planet stage. The reason for this difference is illustrated in figure 14, which shows the results of analytically predicted power loss per planet. Both planetaries were operating at the same speed, same lubrication parameters, and same torque carried per planet. The power loss from the spherical planet bearings (fig. 14(a)) was much greater than the losses from the cylindrical planet bearings and in fact was greater than the

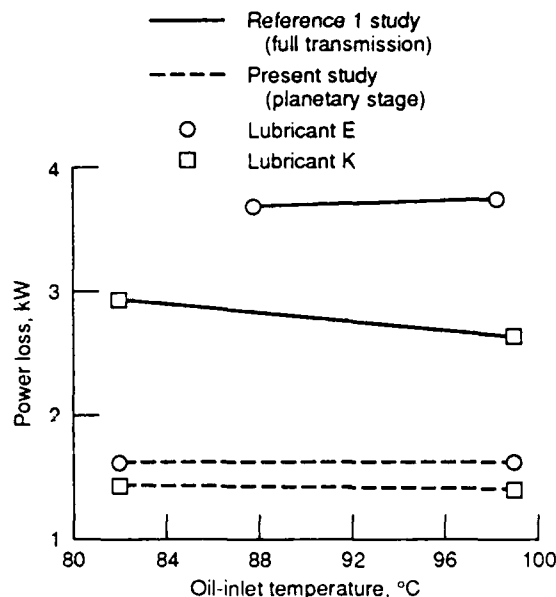


Figure 15.—Comparison of planetary with full transmission (power loss versus oil-inlet temperature).

loss from the entire four-planet planetary stage. This large power loss is due to the great amount of sliding that occurs in the double-row spherical bearings (ref. 17).

Comparison with reference 1.—Reference 1 reports the results of experiments done to measure the efficiency of a complete OH-58 helicopter transmission using several lubricants. The planetary stage used in the transmission tested in reference 1 was identical to the planetary stage of the present study, and two of the lubricants tested in reference 1 were lubricants E and K. The experimental results of the two studies are compared in figure 15. In both studies the power loss with lubricant E was greater than that with lubricant K. The data of figure 15 also show that the planetary loss was approximately 45 to 55 percent of the total transmission power loss for this transmission.

Summary of Results

Experimental and analytical studies were done on the efficiency of a helicopter transmission planetary stage. Parametric studies were done to experimentally determine the effect of operating conditions on the efficiency of a planetary stage. The measured efficiency over all test variables ranged from 98.64 to 99.83 percent. The efficiency of the planetary stage was also studied analytically. Two different analytical models for calculating power loss due to oil displacement from the gear mesh were investigated. The results of the experiments and the analysis were compared with each other and with results of other investigators. The following specific results

were obtained:

1. The analysis predicted higher efficiencies than were experimentally measured. The best correlation between analytical and experimental results was for the lowest lubricant inlet temperature studied.

2. The analysis predicted a higher efficiency for lubricant K than for lubricant E and also predicted that the efficiency would increase as torque was decreased. The experimental results showed the same trends.

3. The analysis predicted that efficiency would increase as speed was decreased. The experimental results, however, showed that efficiency sharply decreased as speed was decreased.

4. Analysis of fluid flow from meshing gear teeth showed that inertia effects were more significant than viscous effects.

5. Including the oil displacement loss model in the analysis improved the correlation of experiments and analysis. The reason for the difference between experimental and analytical results was not determined.

6. The results of the present study were compared with those of a previous study of a similar planetary stage. One stage was found to be much more efficient than the other. The reason for this is that there was a much greater power loss from the spherical bearings used in the three-planet planetary than from the cylindrical bearings used in the four-planet planetary. For the three-planet planetary the efficiency was better for lubricant K than lubricant E; for the four-planet planetary the efficiency was better for lubricant E.

7. The results of the present study were compared with those of a previous study of a complete helicopter transmission that included the same planetary stage as the present study. The comparison showed that the planetary loss was about 45 to 55 percent of the total transmission power loss.

Lewis Research Center
National Aeronautics and Space Administration
Cleveland, Ohio, July 2, 1990

Appendix—Application of Equation (1)

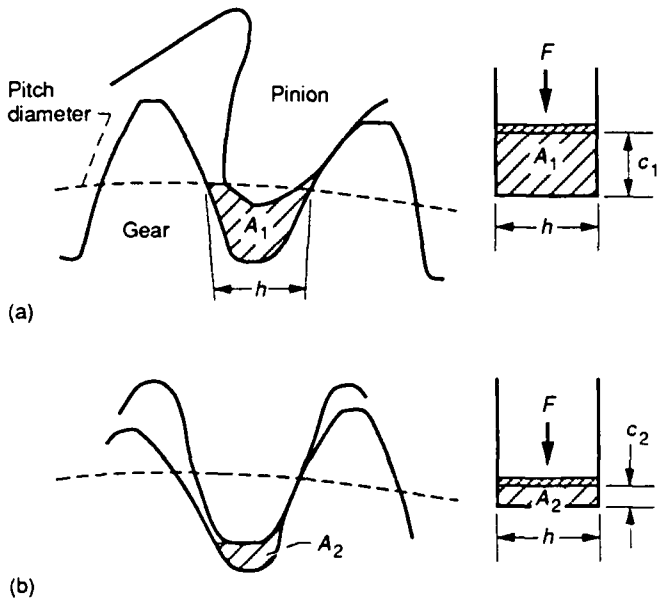
Equation (1) is a formula for calculating the work done to displace oil from the model shown in figure 5. The equation is

$$W = \int_{c_1}^{c_2} \frac{b^3 h \mu}{c^3} \frac{dc}{dt} dc \quad (1)$$

where

- c height of channel
- b length of channel
- h width of channel
- μ absolute viscosity of fluid
- dc/dt velocity of plate

In order to apply this equation and predict oil displacement losses in a gear mesh, all of the terms in the equation must be related to the gears in such a way that the fluid flow from the model represents the fluid flow from the gear mesh. The term b was set equal to the face width of the gear. The term h was set equal to the distance between adjacent gear teeth at the pitch diameter (fig. 16), and the term μ was set equal to the oil viscosity at the average of the oil-inlet and oil-outlet temperatures.



(a) Gears and model at start of analysis.

(b) Gears and model at end of analysis.

Figure 16.—Application of oil displacement model.

In order to simulate fluid flow from the gear mesh, the area available for flow from the model was set equal to the area available for flow from the gears. The area available for flow from the gears as a function of angular position of the pinion was determined by using oversized cardboard models of the gears. The trapped area in the gear mesh at several angular positions was determined, and the data were fit to a second-order polynomial. In order for the areas available for flow from the gears and the model to be equal, the term c in equation (1) must be selected so that

$$c = \frac{A}{h} \quad (A1)$$

where

- c height of plate above channel
- h width of channel
- A area available for flow from gear mesh

In order to define the term dc/dt in equation (1), equation (A1) was differentiated to yield

$$\frac{dc}{dt} = \frac{1}{h} \left(\frac{dA}{d\theta} \frac{d\theta}{dt} \right) = \frac{\dot{\theta}}{h} \frac{dA}{d\theta} \quad (A2)$$

where

- $\dot{\theta}$ angular velocity of pinion
- $dA/d\theta$ rate of change of flow area with respect to angular position of pinion

The limits of the integral of equation (1), c_1 and c_2 , were found by applying equation (A1) first when the tip of the invading tooth crossed the pitch diameter of the mating gear to calculate c_1 and again when the flow area was minimum to calculate c_2 (fig. 16). This implies that the amount of oil trapped is just enough to fill the trapped area when the tip of the invading tooth crosses the pitch diameter of the mating gear.

All of the terms in equation (1) having been defined, the integration was carried out numerically. The result of the calculation was the work done by the force acting on the plate as the oil was displaced from the channel. Since the flow from the model simulates flow from the gear mesh, the result also represents the work done by the gears to displace oil from the mesh during one mesh cycle.

References

1. Mitchell, A.M.; and Coy, J.J.: Lubricant Effects on Efficiency of a Helicopter Transmission. Problems in Bearings and Lubrication, AGARD CP-323, AGARD, Paris, France, 1982, pp. 20-1 to 20-16. (Also NASA TM-82857.)
2. Ariura, Y., et al.: The Lubricant Churning Loss in Spur Gear Systems. Bull. JSME, vol. 16, no. 95, May 1973, pp. 881-892.
3. Mizutani, H.; Isikawa, Y.; and Townsend, D.P.: Effects of Lubrication on the Performance of High Speed Spur Gears. NASA TM-101969, 1989.
4. Handschuh, R.F.; and Rohn, D.A.: Efficiency Testing of a Helicopter Transmission Planetary Reduction Stage. NASA TP-2795, 1988.
5. Coy, J.J.; Mitchell, A.M.; and Hamrock, B.J.: Transmission Efficiency Measurements and Correlations With Physical Characteristics of the Lubricant. Gears and Power Transmission Systems for Helicopters and Turboprops, AGARD CP-369, AGARD, Paris, France, 1984, pp. 20-1 to 20-15. (Also NASA TM-83740.)
6. Anderson, N.E.; Lowenthal, S.H.; and Black, J.D.: An Analytical Method To Predict Efficiency of Aircraft Gearboxes. AIAA Paper 84-1500, June 1984. (Also NASA TM-83716.)
7. Anderson, N.E.; and Lowenthal, S.H.: Spur-Gear-System Efficiency at Part and Full Load. NASA TP-1622, 1980.
8. Anderson, N.E.; and Lowenthal, S.H.: Efficiency of Nonstandard and High Contact Ratio Involute Spur Gears. J. Mechanisms Transmission Automation Design, vol. 108, no. 1, Mar. 1986, pp. 119-126. (Also NASA TM-83725.)
9. Ishibashi, A.; and Yoshino, H.: Power Transmission Efficiencies and Friction Coefficients at Teeth of Novikov-Wildhaber and Involute Gears. ASME Paper 84-DET-58, Oct. 1984.
10. Martin, K.F.: The Efficiency of Involute Spur Gears. J. Mech. Des., vol. 103, no. 1, Jan. 1981, pp. 160-169.
11. Mitchell, A.M.; Oswald, F.B.; and Schuller, F.T.: Testing of YUH-61A Helicopter Transmission in NASA Lewis 2240-kW (3000-hp) Facility. NASA TP-2538, 1986.
12. Dally, J.W.; Riley, W.F.; and McConnell, K.G.: Instrumentation for Engineering Measurements. John Wiley & Sons, Inc., 1984, pp. 543-545.
13. Kleckner, R.J.; Pirvics, J.; and Ragen, M.A.: Spherical Roller Bearing Analysis. SKF Computer Program SPHERBEAN, Vol. 1: Analysis. NASA CR-167858, 1982.
14. Kleckner, R.J.; Dyba, G.J.; and Ragen, M.A.: Spherical Roller Bearing Analysis. SKF Computer Program SPHERBEAN, Vol. 2: User's Manual. NASA CR-167859, 1982.
15. Tevaarwerk, J.L.: Constitutive Modelling of Lubricants in Concentrated Contacts at High Slide to Roll Ratios. (IR-4, Transmission Research Inc.; NASA Contract DEN3-35.) NASA CR-175029, 1985.
16. Pechersky, M.J.; and Wittbrodt, M.J.: An Analysis of Fluid Flow Between Meshing Spur Gear Teeth. 1989 International Power Transmission and Gearing Conference, Vol. 1, American Society of Mechanical Engineers, 1989, pp. 335-342.
17. Kleckner, R.J.; and Pirvics, J.: Spherical Roller Bearing Analysis. J. Lubr. Technol., vol. 104, no. 1, Jan. 1982, pp. 99-108.



NASA
National Aeronautics and Space Administration

Report Documentation Page

1. Report No. NASA TP-3063 AVSCOM TR-90-C-001		2. Government Accession No.		3. Recipient's Catalog No.	
4. Title and Subtitle Experimental and Analytical Evaluation of Efficiency of Helicopter Planetary Stage				5. Report Date November 1990	
				6. Performing Organization Code	
7. Author(s) Timothy L. Krantz				8. Performing Organization Report No. E-5268	
				10. Work Unit No. 505-63-51 1L16221147A	
9. Performing Organization Name and Address NASA Lewis Research Center Cleveland, Ohio 44135-3191 and Propulsion Directorate U.S. Army Aviation Systems Command Cleveland, Ohio 44135-3191				11. Contract or Grant No.	
				13. Type of Report and Period Covered Technical Paper	
12. Sponsoring Agency Name and Address National Aeronautics and Space Administration Washington, D.C. 20546-0001 and U.S. Army Aviation Systems Command St. Louis, Mo. 63120-1798				14. Sponsoring Agency Code	
15. Supplementary Notes					
16. Abstract <p>The efficiency of a helicopter transmission planetary stage was studied both experimentally and analytically. Experiments were done by using a back-to-back, test-and-slave arrangement. The experiments were a parametric study of the effects of operating conditions on efficiency. In order to enhance the analysis, a model was developed that calculates the power required for the meshing gears to displace oil trapped between the gear teeth. In general, the analysis predicted higher efficiencies than were measured. The results of this study were compared with those of other studies.</p>					
17. Key Words (Suggested by Author(s)) Gears Transmissions Efficiency Power loss			18. Distribution Statement Unclassified - Unlimited Subject Category 37		
19. Security Classif. (of this report) Unclassified		20. Security Classif. (of this page) Unclassified		21. No. of pages 20	
				22. Price* A03	